DOI: 10.24996/ijs.2024.65.12.41

ISSN: 0067-2904

Using the Multi-Temporal Landsat Data for Detecting Land Cover Change in Nampula City, Mozambique

Augusto Vundo[1]*, Almaz Akhmetov[2], Hesborn Ondiba[3]
[1]*Faculty of Geosciences, Rovuma University, Nampula, Mozambique*
[2]*Institute of Systems and Information Engineering, University of Tsukuba, Tsukuba, Japan*
[3]*School of Biosystems and Environmental Engineering (SoBEE), Jomo Kenyatta University of Agriculture and Technology, Nairobi, Kenya*

Received: 30/5/2023 Accepted: 24/10/2023 Published: 30/12/2024

Abstract

The change in land cover eventually occurs as the population increases, resulting in high human activities. Monitoring this change can be beneficial for territorial planning and ecosystem monitoring. Therefore, this study aimed to evaluate the spatial-temporal patterns and rates of land cover change in Nampula City, Mozambique, over the past three decades (1989-2020). For this purpose, data from the Landsat-5 TM and Landsat-8 OLI / TIRS satellites were applied as input to two classification systems: (1) thresholding-NDVI and MNDWI and (2) supervised classification. The results showed that the supervised classification method performed better than the thresholding system, with an overall accuracy of 92.4% and a kappa coefficient of 0.89. Estimates pointed to a reduction of 0.04% in the water area and 20.3% in cultivated land. In contrast, barren rock and urban areas experienced an increase of 18.2%, while shrubs and grasslands showed a growth of 2.1% of their area. The results showed a considerable change over the study period and that the spatial dynamics of crop and barren rock and urban areas resulting from human interventions require special consideration. This study provides an opportunity for further studies on the spatial dynamics of land cover change in Nampula City, facilitating effective land management and sustainable development strategies in the region.

Keywords: Remote Sensing, Land Cover, NDVI, MNDWI, Supervised Classification, Nampula.

1. Introduction

The increase in population and density always triggers pressure on natural resources and changes in land use over time. As a result, land cover may change, which includes loss of vegetation, expansion of urban areas, desertification, and reduction of water area, to name a few. According to Lambin et al. [1], land cover is the attribute of the land surface, such as vegetation, water, desert, ice, and other cover resulting from human activities.

Environmental and landscape changes are primarily the result of human activity, such as an increase in the impervious surface area [2] [3]. Lambin et al. [1] highlighted the complexity of understanding land use/cover change in tropical regions. The study suggested conducting a systematic analysis of land-use change at the local scale on a time scale to help uncover the general principles for predicting future changes. Although the phrases “land use”

*Email: nunesvundo2@yahoo.co.uk

and “land cover” are often used interchangeably, it should be noted that land cover is the vegetation and artificial constructions that cover the land surface [4].

Remote sensing techniques are considered time-efficient for consistent spatial and temporal assessment of land cover changes [5] [6]. The Normalized Difference Vegetation Index (NDVI) is among the indices calculated from satellite remote sensing data. This index is applied to determine the amount of healthy vegetation in a site, depending on its density [7] [8]. The Normalized Difference Water Index (NDWI), later known as the Modified Normalized Difference Water Index (MNDWI), is another frequently used index for extracting water, which is effective in accurately discriminating water from non-water resources [9] [10] [11]. NDVI and MNDWI were selected due to their sensitivity to distinct surface characteristics and effectiveness in remote sensing applications. The NDVI can apply to various vegetation types, including forests, grasslands, and crops. Different vegetation types show distinct NDVI signatures, enabling differentiation between land cover classes, while the MNDWI is specifically designed to detect water bodies, making it a reliable index for tracking changes in aquatic features [8] [10]. Therefore, using the NDVI to monitor changes in vegetation cover alongside MNDWI to detect alterations in water bodies provides a comprehensive understanding of environmental changes. Phiri and Morgenroth [12] reviewed developments in cover classification methods and found that all classification methods applied to Landsat images had strengths and limitations, ranging from selecting the correct training samples to using a suitable Landsat image. Despite their limitations, Landsat images are often used in land cover mapping studies [2] [5] [13]. In addition, Landsat data are freely available, with multi-spectral and multi-temporal composition, and provide a source of information for environmental monitoring [2]. Despite the benefits and applications, the products derived from the program have not been widely used to monitor land cover changes at the local level in Mozambique.

Following the Civil War in Mozambique, efforts primarily concentrated on infrastructure development and reconstruction of the country rather than considering the impacts of economic development and other human activities on the environment, including documenting temporal environmental changes. Consequently, there exists a gap in the available information on land cover maps at the local or regional level with medium to high spatial resolution in Mozambique. Therefore, this study aims to examine the spatiotemporal distribution of different land covers using satellite images from Landsat-5 TM (Thematic Mapper) and Landsat-8 OLI (Operational Land Imager) covering the period from 1989 to 2020 [14] [15]. Considering that land cover change in the city of Nampula has not been comprehensively studied, the objectives of this study were: (1) to create land cover maps using NDVI and MNDWI through thresholding and Supervised Classification using Maximum Likelihood Classification (MLC), (2) to compare the performance of each classification method (3) to estimate patterns of spatiotemporal land cover change.

2. Methodology

2.1 Study Area

The city of Nampula is located in the central part of Nampula Province between 15°06’59’’S and 39°15’60’’E. Encompassing an approximate area of 329.81 km², the city rests at an average elevation of 258 m above sea level (refer to Fig. 1). Utilizing the Global multi-resolution terrain elevation data 2010 (GMTED2010) [16], an analysis was conducted to determine the distribution of the city’s area across various altitude ranges. The GMTED2010 dataset, designed for global and continental scale applications, increases the accuracy of global topographic data, making it suitable for worldwide and continental use. Part of the city is between 279-408 m (58%) and (10%) above 408 m. Hills and plateaus

characterize the topography surrounding Nampula City. In terms of climate, the average daily temperature is around 31°C, accompanied by high humidity levels. The city has a rainy season from December to March. As of 2017, the city's population, as reported by the National Institute of Statistics [17], stood at 666,212 residents, making it the third most populous city in the country at that time.

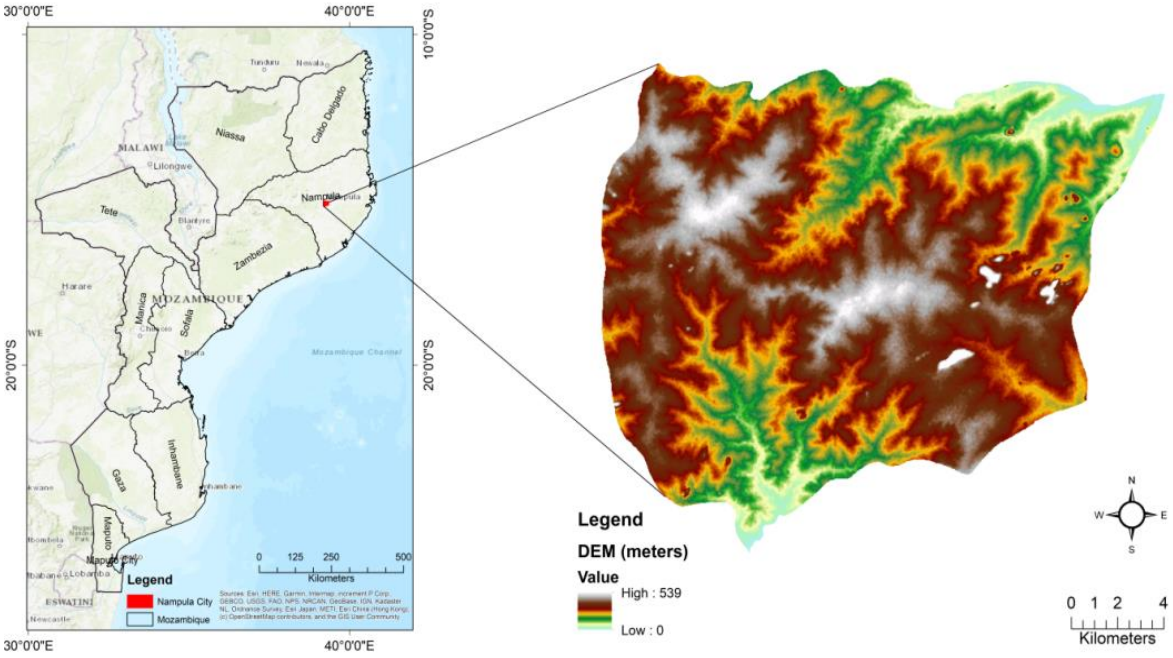

Figure 1: Study area based on 2010 Global Multi-resolution Terrain Elevation Data (GMTED-2010)

2.2 Image Pre-processing

According to the Landsat-Earth Observation Satellites Program [18] and Wulder et al. [19], the Landsat program's sensors have evolved, bringing advancements in capabilities, image quality, and data acquisition. The Multispectral Scanner (MSS) on Landsat Satellites 1 to 5 provided the first set of sensors for Earth observation. The Thematic Mapper (TM) on Landsat Satellites 4 and 5 introduced an improved spatial resolution of 30 meters and an additional thermal band for land surface temperature estimation. However, further improvements were made, like the Enhanced Thematic Mapper Plus (ETM+), featured on Landsat Satellite 7, enhancing radiometric and geometric accuracy. Including an onboard Scan Line Corrector (SLC) reduced data gaps arising from sensor malfunctions. This was succeeded by the Operational Land Imager (OLI) and Thermal Infrared Sensor (TIRS) on Landsat 8, which offered nine bands, including a panchromatic band, visible, near-infrared, and thermal infrared bands. This sensor marked a significant advancement with an improved spatial resolution of 15 meters for some bands, a more comprehensive spectral range, and enhanced accuracy in thermal infrared measurements. Landsat 9 continued this trajectory with similar spectral bands to Landsat 8, incorporating OLI and TIRS sensors. Despite inherent limitations, Landsat data remains an invaluable resource for researchers, scientists, and decision-makers.

The Landsat data used was obtained free of charge from the United States Geological Survey-USGS website [20] in the dry season of 1989 and 2020 (Table 1). Due to the large size of the Landsat data, only one scene (path/raw (165/70)) was needed. All images were reprojected for Geographical Projection and WGS 1984 Ellipsoid Datum Geocentric. Only

clear images were used with cloud cover equal to or less than 5% for the entire Landsat scene, not affecting the study area. Landsat data bands have different spatial resolutions, so the study used the Landsat-5 and Landsat-8 OLI multispectral bands with a spatial resolution of 30 m [21]. Satellite images were subsets for the study area using a shapefile in ENVI 5.2, individually converted from digital number (DN) to radiance and reflectance, and then stuck in a layer to calculate spectral indices and further processing and mapping using ArcGIS 10.2.

Table 1: Characteristics of Landsat data selected for the study

Date Acquired	Satellite	Sensor	Path /Row	Spatial Resolution (m)	Wavelength (μm) Range	Cloud cover (%)
1989-10-23	Landsat 5	TM (Thematic Mapper)	165/70	30	0.45-1.75	5.00
2020-09-26	Landsat 8	OLI (Operational Land Imager) and TIRS (Thermal Infrared Sensor)	165/70	30	0.45-1.65	0.01

The bands were radiometrically corrected from the original DN to spectral radiance using Equation 1 for Landsat-5 [22] and Equation 2 for Landsat-8 [23] [24]. Conversion to spectral radiance was performed using the radiance scale factors provided in each image's metadata file.

$$L_\lambda = \left(\frac{LMAX_\lambda - LMIN_\lambda}{Q_{calmax}}\right) Q_{cal} + LMIN_\lambda \quad (1)$$

$$L_\lambda = ML * Q_{cal} + A_L \quad (2)$$

Where L_λ is the spectral radiance in (W/(m^2 * sr * μm)); $LMAX_\lambda$ is the maximum radiance of the Top Of Atmosphere (TOA) in (W / (m^2 * sr * μm)); $LMIN_\lambda$ is the minimum TOA radiances in (W / (m^2 * sr * μm)); Q_{cal} is the Level 1 pixel value in DN; Q_{calmax} is the maximum DN (65535 for 16-bit Landsat-8 and 255 for Landsat-5); ML is the multiplicative radiance scale factor for the band, and A_L is the additive radiance scale factor for the band.

The data were transformed into TOA reflectance after converting from DN to spectral radiance. To ensure data consistency and reduce scene variability, practices like normalizing solar irradiance and converting spectral radiance into top-of-atmosphere (TOA) reflectance are recommended, as suggested by Chander and Markham [25] and Chander et al. [22]. This normalization process can enhance the usability and reliability of Landsat data for accurate analysis and interpretation. Therefore, radiance data was converted to surface reflectance using Equation 3:

$$\rho p = \frac{\pi * L_\lambda * d^2}{ESUN_\lambda * COS\theta_s} \quad (3)$$

Where ρp is the unitless planetary reflectance; L_λ is the spectral radiance at the sensor aperture. The d represents the earth-sun distance in astronomical units. The Earth-Sun distance, an astronomical unit (AU), is approximately 152.09 million km = 1 au. This value is considered a constant and is used as a fundamental unit of measurement in astronomy to describe distances within the solar system; $ESUN_\lambda$ is a mean of the solar exoatmospheric irradiances; θ_s is the solar zenith angle in degrees.

2.3 Calculation of the Landsat Spectral Index from Surface Reflectance

To obtain the NDVI and MNDWI, the surface reflectance derived from the previous processing step (Equation 3) into Equations 4 and 5 was incorporated. The NDVI, which utilizes the near-infrared and red bands, primarily reflects the presence of vegetation. A higher NDVI value indicates denser and healthier vegetation. On the other hand, the MNDWI [10] significantly enhances the identification of open water characteristics and effectively distinguishes water from non-water areas. Employing the MNDWI can more accurately capture water bodies and differentiate them from other features in the landscape [10].

$$\text{NDVI} = \frac{(NIR - Red)}{(NIR + Red)} \quad (4)$$

$$\text{MNDWI} = \frac{(Green - SWIR)}{(Green + SWIR)} \quad (5)$$

NIR is the near-infrared band; Red and Green are the red and green bands, respectively; SWIR is the short-wave infrared band. These bands were channeled to positions 2 (Green), 3 (Red), 4 (NIR), and 5 (SWIR) for Landsat-5 and 3, 4, 5, and 6 for Landsat-8.

2.4 Image classification system

The study applies two image classification systems: (1) thresholding and (2) supervised classification. The thresholding technique was applied to NDVI and MNDWI images. The unique characteristics of each land cover were identified using high-resolution images from Google Earth Pro and basic statistics results from ENVI 5.2 software in NDVI and MNDWI. Classes were defined using the information and the basic statistics in Table 2 by considering their values, frequency, and pixel distribution within the data. As a result, the thresholds presented in Table 3 were obtained (compared to the USGS), along with the corresponding land cover classes described in Table 4. To estimate the land cover classes, the supervised classification was employed using its widely used Maximum Likelihood Classifier algorithm to estimate the land cover classes. In order to achieve the classification, Google Earth images were used as a reference, and different combinations of bands were used to help identify the different classes to define the training data through polygon delineation to create various regions of interest. The temporal changes in the values of each index are particularly evident in the mean, Table 2. From 1989 to 2020, there was a decrease in the mean values of 0.4 in the NDVI and -0.1 in the MNDWI. Likewise, differences were found in the maximum and minimum values.

Table 2: The statistical description of NDVI and MNDWI in the study area

	NDVI		MNDWI	
	1989	2020	1989	2020
Min	-0.35	-0.22	-0.69	-0.87
Max	0.75	0.70	0.79	0.59
Mean	0.30	0.26	-0.44	-0.45
StdDev	0.09	0.07	0.05	0.07

Table 3: Index thresholding

Index	Land Cover	USGS_Brown	1989	2020	Index	1989	2020
NDVI	Water	---------	≤ -0.00	≤ -0.00	MNDWI	≥ 0.00	≥ 0.00
	Barren rock and urban	< 0.15	>-0.00 ≤ 0.20	> -0.00 ≤ 0.18		> -0.30 ≤ -0.00	> -0. 40 ≤ -0.00
	Shrubs and grasslands	≥ 0.15 < 0.50	>0.20 ≤ 0.50	>0.18≤0.40		≥ -0.69 ≤ -0.40	≥ -0.87 ≤ -0.49
	Crop	≥ 0.50 ≤ 0.90	> 0.5	>0.40		> -0.40 ≤ -0.30	> -0.49 ≤ -0. 40

In Table 3, an NDVI value of negative zero implies an absence of vegetation and corresponds to a water-covered area. On the other hand, a value of positive zero obtained from MNDWI means the detection of water bodies within the observed region. Our study's threshold values align closely with those the US Geological Survey (USGS) suggested. Considering the distinct attributes of the study location, such as elevation, precipitation, solar exposure, and soil moisture, these newly established threshold values were adopted for categorizing different land cover classes. The land cover classes based on the threshold classification scheme are detailed in Table 4.

Table 4: Description of land cover classes

Class	Description
Water	Lakes, permanent ponds, rivers, and streams.
Barren rock and urban land	All impervious surfaces, including rocky mountains and hills and sandy areas.
Shrubs and grasslands	Sparse vegetation, grass, shrubs.
Crop	Vegetables at their peak growth stage (cabbage, lettuce, kidney beans, maize).

2.5 Accuracy Assessment

Following the classification of the images, an accuracy assessment process was performed. According to Olofsson et al. [26], there must be reference data to validate the estimates from the satellite data. Ideally, the reference data should be significantly more accurate than the map classification derived from satellite imagery, and the most accurate source of information should come from ground observations [26] [27]. However, due to various constraints in collecting such data, visual observations from aerial or satellite imagery were used for assessment purposes. Based on these considerations, the validation approach involved 706 randomly collected sample data from Google Earth images. This method holds scientific merit due to its well-documented effectiveness in prior remote sensing and land cover studies. Similar validation strategies have been employed by Vivekananda et al. [28] and Stehman [29] in their investigations of land cover classifications. By adhering to this established procedure, the robustness of our findings and contribution to the methodological consistency that advances the broader scientific understanding of land cover assessment through remote sensing techniques were enhanced [26] [27].

$$\text{PA} = \frac{\text{Total no. of correctly classified samples in each category}}{\text{Total no.of correctly classified samples in that category(col total)}} * 100 \quad (6)$$

$$UA = \frac{\text{Total no. of correctly classified samples in each category}}{\text{Total no. of correctly classified samples in that category(row total)}} * 100 \quad (7)$$

$$OA = \frac{\text{Total no. of correctly classified samples}}{\text{Total no. of reference samples}} * 100 \quad (8)$$

$$KC = \frac{[(\text{Total sum of correct}) - \text{sum of all(col total} * \text{row total})]}{[(\text{Total sum of correct})^2 - \text{sum of all(col total} * \text{row total})]} \quad (9)$$

The implementation of an error matrix and the calculation of metrics such as producer's accuracy (PA), user's accuracy (UA), overall accuracy (OA), and the kappa coefficient (KC) align with well-established standards for accuracy assessment. Furthermore, Equation 6-9, as detailed in previous works by Alam et al. [30], Olofsson et al. [26], and Vivekananda [28], provides a robust framework for summarizing the accuracy assessment outcomes. This approach ensures the reliability and validity of our accuracy assessment methodology, aligning with the best practices outlined by previous studies in the field.

3. Results and discussion

Based on the initial MNDWI and NDVI results, both the 1989 and 2020 datasets indicate that areas with high and low values of each index are primarily concentrated in the central region. This observation becomes evident when examining the distribution of the MNDWI thematic maps (a) for 1989 and (b) for 2020, alongside the NDVI thematic maps (c) for 1989 and (d) for 2020. In these thematic maps, the central region consistently exhibits lower values of NDVI, suggesting an absence or poor health of vegetation. These findings are illustrated in Fig. 2.

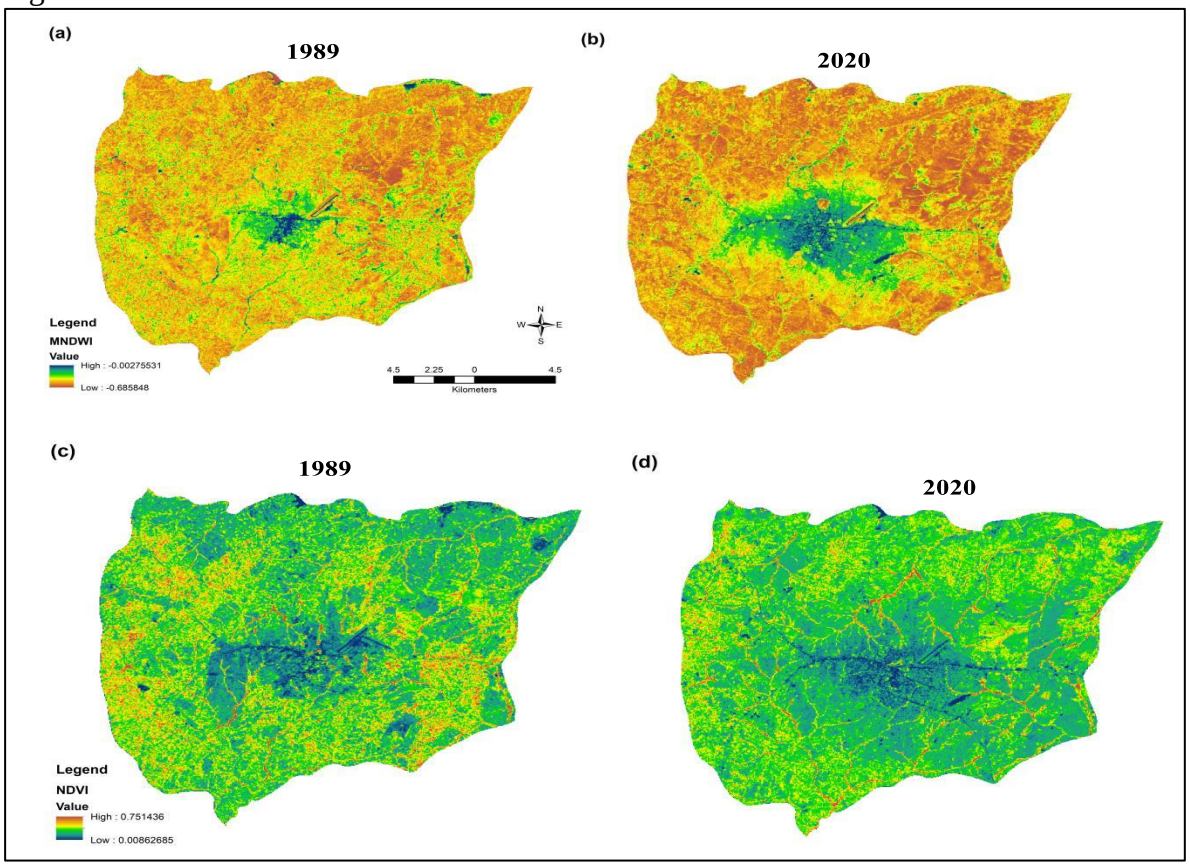

Figure 2: MNDWI maps (a-1989, b-2020) and NDVI maps (c-1989, d-2020)

The threshold and Maximum Likelihood Classification (MLC) analysis results demonstrated stability and a slight decrease in the water area. Contrarily, the barren rock and

urban areas exhibited an increase of 15.6%, 0.7%, and 18.2% for the Modified Normalized Difference Water Index (MNDWI), Normalized Difference Vegetation Index (NDVI), and MLC, respectively.

Regarding the shrubs and grasslands, the NDVI thresholding scheme was reduced by 3.3%, and the MNDWI showed a significant decrease of 54.2%. However, the MLC approach showed an increase of 2.1% in this class. In contrast, the cropland area displayed an increase in both NDVI (2.6%) and MNDWI (38.6%) using the threshold mechanism, while the MLC analysis indicated a decrease of approximately 20.3% in the cropland area (refer to Fig. 3 and Table 5).

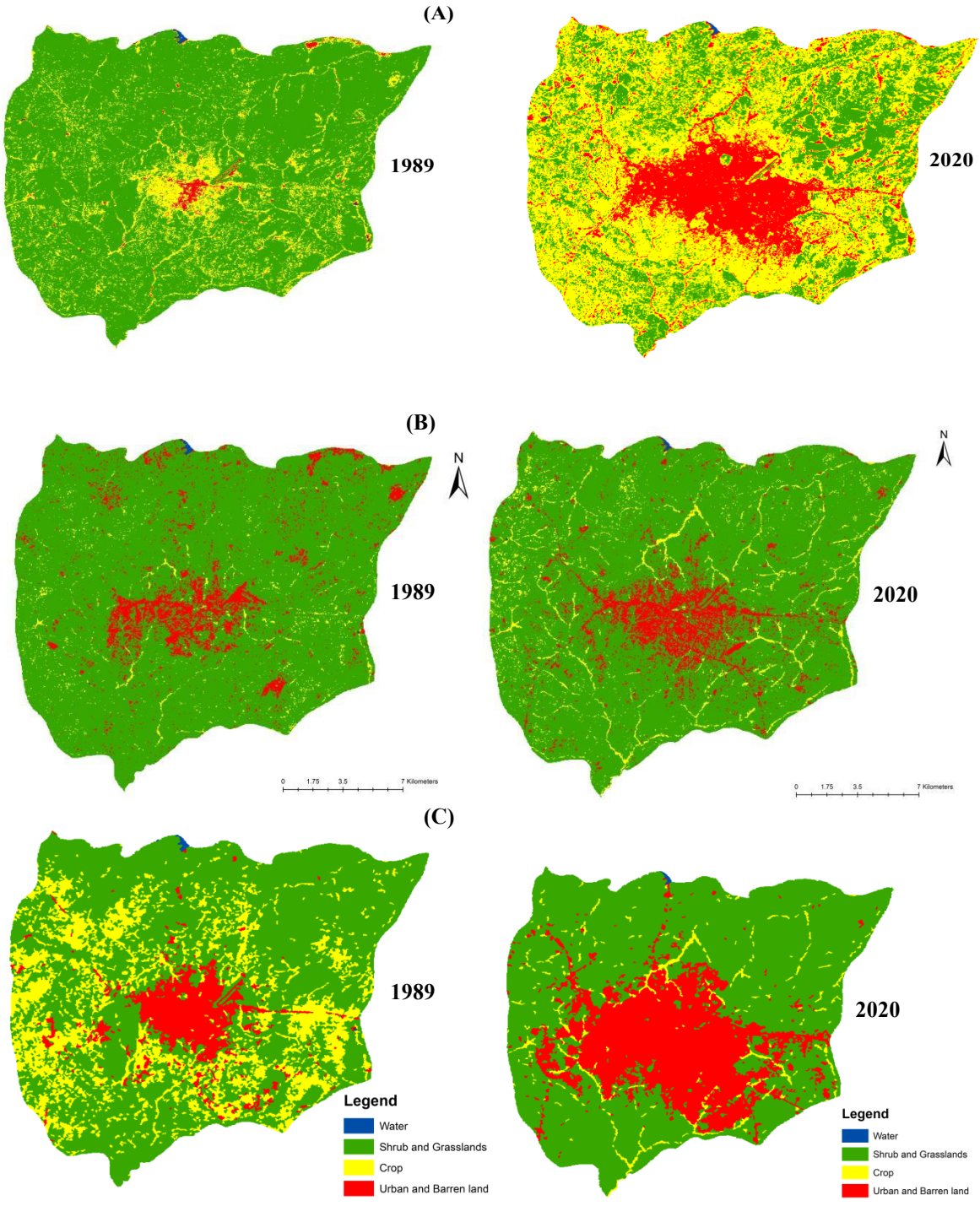

Figure 3: (A) MNDWI_Thresholding maps (1989, 2020), (B) NDVI_Thresholding maps (1989, 2020), and (C) Supervised Classification maps (1989, 2020)

Table 5: The proportion of land cover change indicators from all estimation schemes

	NDVI		MNDWI		Supervised Classification	
	(%)					
	1989	**2020**	**1989**	**2020**	**1989**	**2020**
Water	0.10	0.10	0.10	0.06	0.10	0.06
Barren rock, urban land	9.30	10.00	0.92	16.55	8.00	26.20
Shrubs and grasslands	89.00	85.70	86.95	32.75	68.03	70.14
Crop at their peak growth stage	1.70	4.30	12.03	50.64	23.87	3.61

In the context of remote sensing [26], the assessment of classification models depends heavily on two metrics: User's Accuracy and Producer's Accuracy. These metrics indicate how well a model or classifier can identify and categorize objects. User's Accuracy (UA) measures the model's ability to correctly identify positive instances (i.e., true positives) of a specific class, while Producer's Accuracy (PA) evaluates the model's capability in precisely classifying positive instances without mistakenly including negatives [26] [30]. Combining these metrics with error matrices provides a reliable framework for assessing model performance when an accurate classification is essential. Tables 6 to 8 show the assessment of the maps in Figure 3 as percentages.

Table 6: Error matrix derived from the MNDWI threshold land cover maps

	Water	**Barren rock and urban land**	**Shrubs and grasslands**	**Crop**	**Total (User)**	**UA (%)**
Water	5	0	0	0	5	100
Barren rock and urban land	0	182	18	30	230	79
Shrubs and grasslands	0	13	145	46	204	71
Crop	0	145	31	91	267	34.1
Total (Producer)	5	340	194	167	706	
PA (%)	100	53.5	74.7	54.5		

Table 7: Error matrix derived from the NDVI threshold land cover maps

	Water	**Barren rock and urban land**	**Shrubs and grasslands**	**Crop**	**Total (User)**	**UA (%)**
Water	3	1	0	1	5	60.0
Barren rock and urban land	0	145	85	0	230	63.0
Shrubs and grasslands	0	0	201	3	204	98.5
Crop	0	2	60	205	267	76.8
Total (Producer)	3	148	346	209	706	
PA (%)	100	98.0	58.1	98.1		

Table 8: Error matrix derived from the supervised classification land cover map

	Water	**Barren rock and urban land**	**Shrubs and grasslands**	**Crop**	**Total (User)**	**UA (%)**
Water	4	0	0	1	5	80
Barren rock and urban	0	206	6	18	230	89.57
Shrubs and grasslands	0	7	194	3	204	95.10
Crop	0	0	19	248	267	92.9
Total (Producer)	4	213	219	270	706	
PA (%)	100	96.7	88.6	91.9		

The results of the three estimation maps, Maximum Likelihood Classification (MLC), NDVI Threshold, and MNDWI Threshold, were evaluated. MLC outperformed the other two in individual classes, with an Overall Accuracy (OA) of 92.4%. Furthermore, the MNDWI Threshold could delineate barren rock and urban land cover types, previously acknowledged only for NDVI and other indices, excluding MNDWI [31]. As for the agreement, the kappa coefficient ranged from 0.41 to 0.89, Table 9.

Table 9: Summary of Land Cover Maps Classification Accuracy

Classification Source	Classification Accuracy	
	OA	KC
NDVI_Threshold	78%	0.68
MNDWI_Threshold	59.9%	0.41
Supervised Classification_MLC	92.4%	0.89

The findings of this study indicate that supervised classification using MLC produced the most accurate estimates. Notably, (Fig. 3C) provides evidence of significant changes in land cover in Nampula City from 1989 to 2020. In 1989, a mixture of cropland, shrubland, and grassland characterized a considerable portion of the study area. Water resources were limited, with small ponds in the central region and one in the north. The central part of the city consisted of barren rock and urban land, surrounded by cropland, shrubland, and grassland. At that time, Nampula City did not serve as a primary food source for the rest of the province due to its low soil moisture and high elevation. However, there were a few streams where people utilized fertile land for vegetable production.

Throughout the 31 years, significant changes occurred in the geographical distribution of land cover. Barren rock and urban land stopped being concentrated only in the central part and expanded in all directions, including areas adjacent to main roads, railways, and existing water resources. Consequently, the water area experienced a reduction of 0.1 km^2, while barren rock and urban land increased by approximately 60 km^2. This decrease in water area can be attributed to changes in the streams within production fields due to sedimentation over time, inadequate management practices, and the demand for sand for construction purposes. The sand excavation for the construction, a lucrative activity in the city, intensifies erosion. The growing population has increased the demand for this resource.

On the other hand, the cultivation area became more localized instead of being dispersed throughout the city. By 2020, the cultivated area had reduced significantly and was predominantly found along streams, in contrast to 1989, when cultivated land was scattered across the entire city. The cultivation areas were replaced by other land cover classes, except for water, resulting in a reduction of approximately 66.8 km^2. These findings highlight a deterioration in food security over time in Nampula City. Therefore, the city relies mainly on surrounding districts to meet its population's food needs since its agricultural land has been converted to other land cover classes. Unlike 1989, where shrubs and grasslands were mixed with crop fields, the current scenario exhibits a clear demarcation of land classes. The land cover of the city in 2020 consisted of a mere 0.2 km^2 of water area, 11.9 km^2 of cultivated land, 86.4 km^2 of barren rock and urbanized areas, and 231.3 km^2 of shrubs and grasslands, as indicated in Table 5. As documented in historical records [17], the population growth in Nampula has led to spontaneous urban expansion, the loss of agricultural land, and the depletion of freshwater resources. These changes can be attributed to a combination of factors, including the lack of environmental awareness and the rising economic power of the

population. This dual influence of population growth and economic development has played a crucial role in transforming the city's land cover. Furthermore, the impact of urban expansion on climate change [32] cannot be ignored in the city transformation over the last three decades.

4. Conclusion

The present study was carried out to estimate the spatial-temporal land cover change pattern in Nampula City. The city experienced rapid economic development due to population growth, leading to increased economic activities and infrastructure expansion. Satellite data from Landsat-5 (TM) and Landsat-8 (OLI/TIRS) encompassing 31 years between 1989 and 2020 were used to study land cover change. Three estimation schemes were used: (1) based on thresholding_NDVI, (2) based on thresholding_MNDWI, (3) Supervised Classification_MLC. The results were evaluated using an error matrix, comparing them to 706 reference samples obtained from Google Earth Pro images. The results showed that the Supervised Classification method generated more accurate estimates than the other approaches. The results indicated a significant transformation in land cover over the past three decades. Major changes included extensive loss of agricultural land and water areas, substantial expansion of urban areas in all directions through urban sprawl, and a minimal increase in shrubs and grasslands.

This study successfully generated a comprehensive map illustrating the changes in land cover and their rates over time using Landsat data. The produced map can serve as a valuable reference for future studies, particularly in land management by the municipal council and other government authorities. Improved land use planning and management practices could effectively prevent the loss of agricultural land and minimize unplanned urban sprawl. This procedure must include active participation of the local community to increase environmental awareness of the current changes. Further studies are needed to refine and meticulously identify the relationship between land cover change and the effects of temperature variation in the city. Furthermore, future studies shall include the assessment of the relationship between urbanization and changes in the local climate [33]. Additionally, mobile phone data could validate the results of land cover change and migration in Nampula City [34].

6. Disclosure and conflict of interest

Conflict of Interest: The authors declare no conflicts of interest.

7. Acknowledgements

The authors are grateful to the anonymous reviewers.

References

[1] E. F. Lambin, H. F. Geist and E. Lepers, "Dynamics of Land-Use and Land-Cover Change in Tropical Regions," *Annual Review of Environment and Resources,* vol. 28, pp. 205-241, 2003.

[2] Y. Zhang, I. O. Odeh and E. Ramadan, "Assessment of Land Surface Temperature in Relation to Landscape Metrics and Fractional Vegetation Cover in an Urban/ Peri-urban region using Landsat data," *International Journal of Remote Sensing,* vol. 34, no. 1, pp. 168-189, 2013.

[3] J. A. Foley, R. Defries, G. P. Asner, C. Barford, G. Bonan, S. R. Carpenter, S. F. Chapin, M. T. Coe, G. C. Daily and H. K. Gibbs, "Global Consequences of Land Use," *Science,* vol. 309, no. 5734, pp. 570-574, 2005.

[4] T. M. Burley, "Land Use or Land Utilization?" *The Professional Geographer,* vol. 13, no. 6, pp. 18-20, 1961.

[5] A. K. Hua and O. W. Ping, "The Influence of Land-Use/Land-Cover Changes on Land Surface Temperature: A Case Study of Kuala Lumpur Metropolitan City," *European Journal of Remote*

Sensing, vol. 51, no. 1, pp. 1049-1069, 2018.

[6] N. T. Tien, "Landsat Time-series Images-based Urban Heat Island Analysis: The Effects of Changes in Vegetation and Built-up Land on Land Surface Temperature in Summer in the Hanoi Metropolitan Area, Vietnam," *Environment and Natural Resources Journal,* vol. 18, no. 2, pp. 177-190, 2020.

[7] T. M. Scanlon, J. D. Albertson, K. K. Caylor and C. A. Williams, "Determining Land Surface Fractional Cover from NDVI and Rainfall Time Series for a Savanna Ecosystem," *Geography,* vol. 82, no. 2-3, pp. 376-388, 2002.

[8] T. Carlson and D. A. Ripley, "On the Relation between NDVI, Fractional Vegetation Cover, and Leaf Area Index," *Remote Sensing of Environment,* vol. 62, no. 3, pp. 241-252, 1997.

[9] S. K. McFeeters, "The Use of Normalized Difference Water Index (NDWI) in the Delineation of Open Water Features," *International Journal of Remote Sensing,* vol. 17, no. 7, pp. 1425-1432, 1996.

[10] H. Xu, "Modification of Normalised Difference Water Index (NDWI) to Enhance Open Water Features in Remotely Sensed Imagery," *International Journal of Remote Sensing,* vol. 27, no. 14, pp. 3025-3033, 2005.

[11] A. Roy and A. B. Inamdar, "Multitemporal Land Use Land Cover (LULC) Change Analysis of a Dry Semi-arid River Basin in Western India Following a Robust Multisensory Satellite Image Calibration Strategy," *Heliyon,* vol. 5, no. 4, p. e01478, 2019.

[12] D. Phiri and J. Morgenroth, "Developments in Landsat Land Cover Classification Methods: A Review," *Remote Sensing,* vol. 9, no. 9, p. 967, 2017.

[13] Z. Wang, W. Yao, Q. Tang, L. Liu, P. Xiao, X. Kong, P. Zhang, F. Shi and Y. Wang, "Continuous Change Detection of Forest/Grassland and Cropland in the Loess Plateau of China Using all Available Landsat Data," *Remote Sensing,* vol. 10, no. 11, p. 1775, 2018.

[14] F. Zhang, T. Tiyip, H. Kung, V. C. Johnson, M. Maimaitiyiming, M. Zhou and J. Wang, "Dynamics of Land Surface Temperature (LST) in Response to Land Use and Land Cover (LULC) Changes in the Weigan and Kuqa River Oasis, Xinjiang, China," *Arabian Journal of Geosciences,* vol. 9, p. 499, 2016.

[15] S. Sinha, L. K. Sharma and M. S. Nathawat, "Improved Land-Use/Land-Cover Classification of Semi-arid Deciduous Forest Landscape Using Thermal Remote Sensing," *Egyptian Journal of Remote Sensing and Space Science,* vol. 18, no. 2, pp. 217-233, 2015.

[16] J. J. Danielson and D. B. Gesch, "Global Multi-resolution Terrain Elevation Data 2010 (GMTED2010)," USGS, Sioux Falls, 2011.

[17] National Institute of Statistics, "IV General Census of Population and Housing 2017 (In Portuguese)," National Institute of Statistics, Maputo, 2019.

[18] The U.S. Geological Survey, "Landsat-Earth Observation Satellites," USGS, Reston, 2015.

[19] M. A. Wulder, D. P. Roy, V. C. Radeloff, T. R. Loveland, M. C. Anderson, D. M. Johnson, S. Healey, Z. Z, T. A. Scambos, N. Pahlevan, M. Hansen, N. Golerick, C. J. Crawford, J. G. Masek, T. Hermosilla, J. C. White, A. S. Belward, C. Schaaf and C. E. Woodcock, "Fifty Years of Landsat Science and Impacts," *Remote Sensing of Environment,* vol. 280, p. 113195, 2022.

[20] The U. S. Geological Survey, "EarthExplorer," USGS, 29 May 2023. [Online]. Available: https://earthexplorer.usgs.gov/. [Accessed 29 May 2023].

[21] M. W. Naikoo, M. Rihan, M. Ishtiaque and Shahfahad, "Analyses of Land Use Land Cover (LULC) Change and Built-up Expansion in the Suburb of a Metropolitan City: Spatio-temporal Analysis of Delhi NCR Using Landsat Datasets," *Journal of Urban Management,* vol. 9, no. 3, pp. 347-359, 2020.

[22] G. Chander, B. L. Markham and D. L. Halder, "Summary of Current Radiometric Calibration Coefficients for Landsat MSS, TM, ETM+, and EO-1 ALI Sensors," *Remote Sensing of Environment,* vol. 113, no. 5, pp. 893-903, 2009.

[23] T.-W. Lee, J. H. Lee and Z.-H. Wang, "Scaling of the Urban Heat Island Intensity Using Time-dependent Energy Balance," *Urban Climate,* vol. 2, pp. 16-24, 2012.

[24] V. Ihlen and K. Zanter, Landsat 8 (L8) Data Users Handbook. November 2019, Sioux Falls: USGS, 2019.

[25] G. Chander and B. L. Markham, "Revised Landsat-5 TM Radiometric Calibration Procedures and Postcalibration Dynamic Ranges," *IEEE Transactions on Geoscience and Remote Sensing,* vol. 41, no. 11, pp. 2674-2677, 2003.

[26] P. Olofsson, G. M. Foody, M. Herold, S. V. Stehman, C. E. Woodcock and M. A. Wulder, "Good Practices for Estimating Area and Assessing Accuracy of Land Change," *Remote Sensing of Environment,* vol. 148, pp. 42-57, 2014.

[27] R. E. McRoberts, S. V. Stehman, G. C. Liknes, E. Naesset, C. Sannier and B. F. Walters, "The effects of Imperfect Reference Data on Remote Sensing-assisted Estimators of Land Cover Class Proportions," *ISPRS Journal of Photogrammetry and Remote Sensing,* vol. 142, pp. 292-300, 2018.

[28] G. Vivekananda, R. Swathi and S. AVLN, "Multi-temporal Image Analysis for LULC Classification and Change Detection," *European Journal of Remote Sensing,* vol. 54, no. 2, pp. 189-199, 2020.

[29] S. V. Stehman, "Estimating Area from an Accuracy Assessment Error Matrix," *Remote Sensing of Environment,* vol. 132, pp. 202-211, 2013.

[30] A. Alam, S. M. Bhat and M. M, "Using Landsat Satellite Data for Assessing the Land Use and Land Cover Change in Kashmir Valley," *GeoJournal,* vol. 85, pp. 1529-1543, 2020.

[31] T. A. Chowdhury and S. M. Islam, "Assessing and Simulating Impacts of Land Use Land Cover Changes on Land Surface Temperature in Mymensingh City, Bangladesh," *Environment and Natural Resources Journal,* vol. 20, no. 2, pp. 110-128, 2022.

[32] Y. K. H. Moussa and A. A. Alwehab, "The Urban Expansion Impact on Climate Change for the City of Baghdad," *Iraqi Journal of Science,* vol. 63, no. 11, pp. 5072-5285, 2022.

[33] A. K. Mohammed Ali and F. K. Mashee Al Ramahi, "A Study of the Effect of Urbanization on Annual Evaporation Rates in Baghdad City Using Remote Sensing," *Iraqi Journal of Science,* vol. 69, no. 8, pp. 2142-2149, 2020.

[34] M. K. Alqaysi and S. F. Behadili, "A Review of Flow Migration Through Mobile Networks," *Iraqi Journal of Science,* vol. 63, no. 5, pp. 2243-2261, 2022.